

## Supporting Information

### Synthesis and Characterization of Azaborepin Radical in Solid Neon through Boron-Mediated C–N Bond Cleavage of Pyridine

Xin Xu,<sup>a</sup> Yi-Kang Zhu,<sup>b</sup> Chuan-Ming Dai,<sup>a</sup> Jiaping Xu,<sup>a</sup> Jiwen Jian<sup>ab \*</sup>

<sup>a</sup> *Hangzhou Institute of Advanced Studies, Zhejiang Normal University, 1108 Gengwen Road,*

*Hangzhou, Zhejiang, 311231, China.*

<sup>b</sup> *Xiaoshan Campus, Zhejiang Normal University, 1108 Gengwen Road, Hangzhou, Zhejiang, 311231,*

*China.*

*\*Author to whom Correspondence should be addressed. Email: [jiwenjian@zjnu.edu.cn](mailto:jiwenjian@zjnu.edu.cn)*

**Table S1.** Observed and calculated products infrared absorptions ( $\text{cm}^{-1}$ ) in the reaction of boron atoms ( $^{10}\text{B}$  and  $^{11}\text{B}$ ) with pyridine molecules in solid neon. The calculated IR intensities are listed in parentheses in  $\text{km/mol}$ . The structural optimization and vibrational frequency computation were conducted at the B3LYP/aug-ccpVTZ level.

	Experimental				Calculated			
	$^{10}\text{B}$	$^{11}\text{B}$	$^{15}\text{N}$	D	$^{10}\text{B}$	$^{11}\text{B}$	$^{15}\text{N}$	D
<b>A</b>	1311.3	1311.3	1311.1	1283.0	1345.0 (10)	1345.0 (10)	1344.8 (11)	1312.9 (16)
	1293.9	1277.5	1274.1	1215.6	1308.0 (142)	1290.0 (134)	1288.1 (135)	1239.5 (23)
	1247.8	1244.8	1235.2	1172.2	1261.9 (12)	1261.9 (12)	1249.3 (13)	1177.1 (3)
	973.7	973.7	--	850.5	1011.1 (23)	1011.1 (23)	1011.0 (23)	864.5 (11)
	664.1	663.7	661.3	569.4	691.5 (60)	691.4 (60)	688.2 (64)	650.0 (9)
	609.8	609.8	609.8	468.7	637.9 (29)	637.9 (29)	636.7 (26)	486.9 (35)
<b>B</b>	1131.1	1125.2	1114.2/1111.9	967.4	1160.0 (29)	1157.4 (26)	1151.6 (21)	988.3 (6)
	1010.4	1010.2	--	850.6	1046.5 (11)	1044.9 (10)	1043.5 (9)	874.1 (20)
	891.2	890.8	891.2	798.5	922.5 (18)	918.3 (25)	920.1 (24)	790.9 (1)
	858.2	857.3	858.1	772.3	890.3 (30)	887.7 (23)	889.5 (23)	762.2 (18)
	796.4/789.6	795.5/789.6	788.8/787.4	621.4	828.7 (10)	820.8 (10)	821.8 (11)	626.2 (10)
<b>C</b>	1745.3	1703.3	1736.3	-	1770.8 (48)	1722.8 (51)	1756.1 (46)	1759.5 (47)
	1533.5	1530.8	1529.9	1473.0	1553.5 (40)	1552.7 (40)	1553.0 (38)	1508.1 (48)
	1374.1	1373.2	1371.0	1171.5	1411.2 (12)	1410.1 (13)	1409.2 (10)	1198.3 (13)
	1278.5	1271.9	1278.4	-	1321.8 (78)	1316.3 (70)	1317.2 (76)	1011.4 (7)
	1239.0	1238.2	1238.6	1132.1	1262.1 (18)	1261.5 (19)	1261.7 (20)	1146.5 (23)
	1168.7	1168.2	1169.1	807.2	1191.8 (39)	1191.5 (38)	1190.7 (40)	868.8 (0)
	1137.5	1134.8	1137.2	-	1163.6 (19)	1161.6 (21)	1158.1 (19)	913.0 (5)
	719.5	719.2	719.2	-	738.1 (22)	738.0 (22)	737.9 (22)	573.3 (3)
	638.5	630.7	637.5	606.3	670.3 (30)	660.5 (27)	668.0 (30)	653.2 (28)
609.2	608.9	-	-	616.0 (71)	615.8 (70)	615.8 (72)	457.9 (2)	

**Table S2.** Product infrared absorptions ( $\text{cm}^{-1}$ ) observed in the reaction of boron atoms ( $^{10}\text{B}$  and  $^{11}\text{B}$ ) with isotopic pyridine molecules in solid neon. The boron-11, nitrogen-15, and deuterium isotopic shifts ratio are labeled as  $R_{10/11}$ ,  $R_{14/15}$ , and  $R_{1/2}$ . The structural optimization and vibrational frequency computation were conducted at the B3LYP/aug-ccpVTZ level.

	Experimental				Calculated			
	$^{10}\text{B}$	$R_{10/11}$	$R_{14/15}$	$R_{1/2}$	$^{10}\text{B}$	$R_{10/11}$	$R_{14/15}$	$R_{1/2}$
<b>A</b>	1311.3	1.0000	1.0002	1.0221	1345.0 (10)	1.0000	1.0001	1.0244
	1293.9	1.0128	1.0155	1.0644	1308.0 (142)	1.0139	1.0154	1.0553
	1247.8	1.0000	1.0142	1.0688	1261.9 (12)	1.0000	1.0101	1.0720
	973.7	1.0000	1.0001	1.1453	1011.1 (23)	1.0000	1.0001	1.1696
	664.1	1.0006	1.0042	1.1663	691.5 (60)	1.0001	1.0048	1.0638
	609.8	1.0000	1.0000	1.3010	637.9 (29)	1.0000	1.0019	1.3101
<b>B</b>	1131.1	1.0052	1.0003	1.1692	1160.0 (29)	1.0022	1.0073	1.1737
	1010.4	1.0002	1.0098	1.1879	1046.5 (11)	1.0015	1.0029	1.1972
	891.2	1.0004	1.0066	1.1161	922.5 (18)	1.0046	1.0026	1.1664
	858.2	1.0010	1.0001	1.1112	890.3 (30)	1.0029	1.0009	1.1681
	796.4/789.6	1.0011	1.0091	1.2816	828.7 (10)	1.0096	1.0084	1.3234
<b>C</b>	1745.3	1.0247	1.0103	-	1770.8 (48)	1.0278	1.0084	1.0064
	1533.5	1.0011	1.0002	1.0291	1553.5 (40)	1.0005	1.0003	1.0301
	1374.1	1.0007	1.0023	1.1729	1411.2 (12)	1.0008	1.0014	1.1777
	1278.5	1.0057	1.0008	-	1321.8 (78)	1.0042	1.0035	1.3069
	1239.0	1.0008	1.0003	1.0944	1262.1 (18)	1.0005	1.0003	1.1008
	1168.7	1.0013	1.0003	1.4487	1191.8 (39)	1.0003	1.0009	1.3718
	1137.5	1.0024	1.0003	-	1163.6 (19)	1.0018	1.0047	1.2745
	719.5	1.0004	1.0004	-	738.1 (22)	1.0000	1.0003	1.2875
	638.5	1.0124	1.0016	1.0531	670.3 (30)	1.0148	1.0034	1.0262
	609.2	1.0007	-	-	616.0 (71)	1.0002	1.0003	1.3453

**Table S3.** Calculated vibrational frequencies (unscaled,  $\text{cm}^{-1}$ ) and intensities (in parentheses in  $\text{km/mol}$ ) of the species A. The experimentally observed values for  $^{10}\text{B}(\text{C}_5\text{H}_5\text{N})$  are also listed for comparison. The structural optimization and vibrational frequency computation were conducted at the B3LYP/aug-ccpVTZ level.

$^{10}\text{B}$			$^{11}\text{B}$		
B+C <sub>5</sub> H <sub>5</sub> N	B+C <sub>5</sub> D <sub>5</sub> N	B+C <sub>5</sub> H <sub>5</sub> <sup>15</sup> N	B+C <sub>5</sub> H <sub>5</sub> N	$^{10}\text{B}/^{11}\text{B}$	Experimental
3223.0(2)	2391.0(0)	3223.0(2)	3223.0(2)	1.0000	
3220.3(0)	2382.2(1)	3220.3(0)	3220.3(0)	1.0000	
3215.8(1)	2375.1(0)	3215.8(1)	3215.8(1)	1.0000	
3189.5(9)	2351.4(6)	3189.5(9)	3189.5(9)	1.0000	
3186.7(0)	2351.4(0)	3186.7(0)	3186.7(0)	1.0000	
1630.9(0)	1578.1(2)	1628.9(1)	1630.8(0)	1.0000	
1538.0(1)	1447.6(1)	1538.0(1)	1538.0(1)	1.0000	
1475.7(6)	1332.8(124)	1473.2(3)	1475.3(5)	1.0003	
1394.1(3)	1043.1(0)	1394.1(3)	1394.1(3)	1.0000	
<b>1345.0(10)</b>	<b>1312.9(16)</b>	<b>1344.8(11)</b>	<b>1345.0(10)</b>	1.0000	<b>1311.3</b>
<b>1308.0(142)</b>	<b>1239.5(23)</b>	<b>1288.1(135)</b>	<b>1290.0(134)</b>	1.0139	<b>1293.9</b>
<b>1261.9(12)</b>	<b>1177.1(3)</b>	<b>1249.3(13)</b>	<b>1261.9(12)</b>	1.0000	<b>1247.8</b>
1201.7(2)	882.8(7)	1199.5(5)	1200.0(2)	1.0014	
1121.6(1)	832.3(1)	1120.0(1)	1121.6(1)	1.0000	
1060.9(1)	846.6(2)	1051.2(1)	1060.9(1)	1.0000	
<b>1011.1(23)</b>	<b>864.5(11)</b>	<b>1011.0(23)</b>	<b>1011.0(23)</b>	1.0000	<b>973.7</b>
987.9(3)	956.2(0)	987.3(3)	985.9(3)	1.0020	
965.1(0)	774.4(0)	965.1(0)	965.1(0)	1.0000	
963.4(1)	786.2(0)	963.3(1)	963.4(1)	1.0000	
817.2(1)	749.2(2)	815.6(0)	808.0(1)	1.0114	
789.8(6)	602.1(6)	789.4(6)	789.8(6)	1.0000	
767.9(0)	603.6(0)	767.9(0)	767.9(0)	1.0000	
<b>691.5(60)</b>	<b>650.0(9)</b>	<b>688.2(64)</b>	<b>691.4(60)</b>	1.0001	<b>664.1</b>
645.2(0)	618.5(0)	644.1(0)	645.2(0)	1.0000	
<b>637.9(29)</b>	<b>486.9(35)</b>	<b>636.7(26)</b>	<b>637.9(29)</b>	1.0000	<b>609.8</b>
518.5(0)	505.8(0)	515.4(0)	511.8(0)	1.0132	
410.9(0)	358.4(0)	410.9(0)	410.9(0)	1.0000	
381.2(1)	344.2(2)	375.0(1)	379.9(1)	1.0036	
287.7(22)	280.8(22)	286.6(22)	279.3(21)	1.0298	
155.0(9)	146.2(9)	154.8(9)	152.1(9)	1.0190	

**Table S4.** Calculated vibrational frequencies (unscaled,  $\text{cm}^{-1}$ ) and intensities (in parentheses in  $\text{km/mol}$ ) of the species **B**. The experimentally observed values for  $^{10}\text{B}(\text{C}_5\text{H}_5\text{N})$  are also listed for comparison. The structural optimization and vibrational frequency computation were conducted at the B3LYP/aug-ccpVTZ level.

$^{10}\text{B}$			$^{11}\text{B}$		
B+C <sub>5</sub> H <sub>5</sub> N	B+C <sub>5</sub> D <sub>5</sub> N	B+C <sub>5</sub> H <sub>5</sub> <sup>15</sup> N	B+C <sub>5</sub> H <sub>5</sub> N	$^{10}\text{B}/^{11}\text{B}$	Experimental
3222.8(13)	2406.7(6)	3222.8(13)	3222.8(13)	1.0000	
3203.4(9)	2381.8(5)	3203.4(9)	3203.4(9)	1.0000	
3198.4(5)	2357.8(5)	3198.4(5)	3198.4(5)	1.0000	
3189.4(3)	2351.4(1)	3189.4(3)	3189.4(3)	1.0000	
3182.5(1)	2348.9(0)	3182.5(1)	3182.5(1)	1.0000	
1631.6(10)	1576.8(12)	1631.4(10)	1631.6(10)	1.0000	
1481.4(4)	1418.0(7)	1481.3(4)	1481.1(4)	1.0002	
1345.5(10)	1159.0(2)	1345.0(10)	1345.0(10)	1.0004	
1307.7(0)	1200.6(4)	1307.7(0)	1307.3(0)	1.0003	
1277.6(6)	1106.0(42)	1277.6(6)	1277.3(6)	1.0003	
<b>1160.0(29)</b>	<b>988.3(6)</b>	<b>1151.6(21)</b>	<b>1157.4(26)</b>	<b>1.0022</b>	<b>1131.1</b>
1132.0(6)	971.8(8)	1129.6(7)	1131.7(6)	1.0003	
1081.2(22)	830.7(0)	1078.3(25)	1074.1(23)	1.0066	
<b>1046.5(10)</b>	<b>874.1(20)</b>	<b>1043.5(9)</b>	<b>1044.9(10)</b>	<b>1.0015</b>	<b>1010.4</b>
1003.3(11)	814.4(2)	998.4(12)	1003.0(11)	1.0003	
975.1(2)	910.3(60)	974.1(2)	973.4(1)	1.0017	
953.3(8)	736.9(11)	952.6(9)	952.2(7)	1.0012	
940.2(8)	751.6(0)	937.4(5)	938.7(7)	1.0016	
<b>922.5(18)</b>	<b>790.9(1)</b>	<b>920.1(24)</b>	<b>918.3(25)</b>	<b>1.0045</b>	<b>891.2</b>
<b>890.3(31)</b>	<b>762.2(18)</b>	<b>889.5(23)</b>	<b>887.7(23)</b>	<b>1.0029</b>	<b>858.2</b>
883.4(15)	822.7(2)	876.2(19)	882.2(22)	1.0014	
<b>828.7(10)</b>	<b>626.2(10)</b>	<b>821.8(11)</b>	<b>820.8(10)</b>	<b>1.0096</b>	<b>795.5/789.6</b>
765.8(11)	682.8(2)	764.2(11)	763.4(11)	1.0032	
<b>744.4(22)</b>	<b>723.3(4)</b>	<b>742.9(20)</b>	<b>736.8(21)</b>	<b>1.0104</b>	-
705.4(3)	619.2(9)	698.5(2)	693.8(4)	1.0168	
665.2(8)	653.9(11)	660.0(9)	662.3(7)	1.0044	
524.3(6)	464.5(5)	523.5(6)	520.1(6)	1.0080	
465.8(12)	426.1(14)	464.2(12)	459.8(11)	1.0130	
438.3(0)	384.3(2)	438.2(0)	437.6(0)	1.0016	
405.5(5)	360.4(4)	404.7(5)	397.6(5)	1.0197	

**Table S5.** Calculated vibrational frequencies (unscaled,  $\text{cm}^{-1}$ ) and intensities (in parentheses in  $\text{km/mol}$ ) of the species **C**. The experimentally observed values for  $^{10}\text{B}(\text{C}_5\text{H}_5\text{N})$  are also listed for comparison. The structural optimization and vibrational frequency computation were conducted at the B3LYP/aug-ccpVTZ level.

$^{10}\text{B}$			$^{11}\text{B}$		
B+C <sub>5</sub> H <sub>5</sub> N	B+C <sub>5</sub> D <sub>5</sub> N	B+C <sub>5</sub> H <sub>5</sub> <sup>15</sup> N	B+C <sub>5</sub> H <sub>5</sub> N	$^{10}\text{B}/^{11}\text{B}$	Experimental
3238.1(0)	2393.8(1)	3238.1(0)	3238.1(0)	1.0000	
3173.7(20)	2343.7(14)	3173.7(20)	3173.7(20)	1.0000	
3158.6(24)	2331.4(18)	3158.6(24)	3158.6(24)	1.0000	
3139.8(5)	2311.5(3)	3139.8(5)	3139.8(5)	1.0000	
3120.6(7)	2299.0(3)	3120.6(7)	3120.6(7)	1.0000	
<b>1770.8(48)</b>	<b>1759.5(47)</b>	<b>1756.1(46)</b>	<b>1722.8(51)</b>	<b>1.0278</b>	<b>1745.3</b>
<b>1553.5(40)</b>	<b>1508.1(48)</b>	<b>1553.0(38)</b>	<b>1552.7(40)</b>	<b>1.0005</b>	<b>1533.5</b>
1497.0(5)	1388.3(37)	1496.7(5)	1497.0(5)	1.0000	
1454.6(7)	1309.7(74)	1453.9(7)	1453.7(6)	1.0006	
<b>1411.2(12)</b>	<b>1198.3(13)</b>	<b>1409.2(10)</b>	<b>1410.1(13)</b>	<b>1.0008</b>	<b>1374.1</b>
<b>1321.8(78)</b>	<b>1011.4(7)</b>	<b>1317.2(76)</b>	<b>1316.3(70)</b>	<b>1.0042</b>	<b>1278.5</b>
<b>1262.1(18)</b>	<b>1146.5(23)</b>	<b>1261.7(20)</b>	<b>1261.5(19)</b>	<b>1.0005</b>	<b>1239.0</b>
<b>1191.8(39)</b>	<b>868.8(0)</b>	<b>1190.7(40)</b>	<b>1191.5(38)</b>	<b>1.0003</b>	<b>1168.7</b>
<b>1163.6(19)</b>	<b>913.0(5)</b>	<b>1158.1(19)</b>	<b>1161.6(21)</b>	<b>1.0018</b>	<b>1137.5</b>
1041.2(7)	930.2(6)	1037.7(7)	1040.4(7)	1.0008	
991.0(0)	810.6(0)	991.0(0)	991.0(0)	1.0000	
975.9(0)	800.4(0)	975.8(0)	975.9(0)	1.0000	
919.4(7)	808.8(2)	918.0(5)	919.3(6)	1.0002	
885.3(5)	743.1(14)	884.5(4)	884.8(5)	1.0006	
860.5(2)	688.1(1)	860.3(2)	860.5(2)	1.0000	
852.5(8)	826.6(3)	846.2(8)	849.1(10)	1.0040	
<b>738.1(22)</b>	<b>573.3(3)</b>	<b>737.9(22)</b>	<b>738.0(22)</b>	<b>1.0000</b>	<b>719.5</b>
<b>670.3(30)</b>	<b>653.2(28)</b>	<b>668.0(30)</b>	<b>660.5(27)</b>	<b>1.0148</b>	<b>638.5</b>
<b>616.0(71)</b>	<b>457.9(2)</b>	<b>615.8(72)</b>	<b>615.8(70)</b>	<b>1.0002</b>	<b>609.2</b>
579.2(1)	516.2(31)	579.2(1)	578.3(0)	1.0016	
498.5(28)	471.8(39)	495.4(27)	487.5(29)	1.0226	
479.7(5)	468.4(4)	479.2(5)	469.7(5)	1.0212	
316.6(1)	278.1(2)	316.6(1)	314.5(10)	1.0070	
315.3(10)	309.2(9)	310.8(10)	313.8(1)	1.0049	
110.4(4)	100.0(4)	109.2(4)	110.4(4)	1.0000	

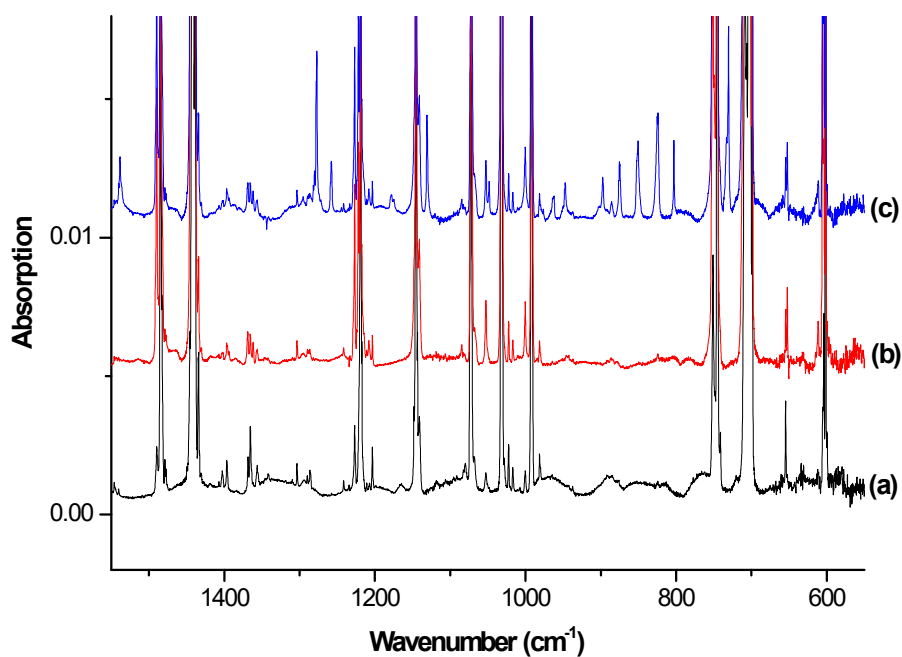


**Figure S1.** Infrared spectra in the  $1550\text{-}550\text{ cm}^{-1}$  region from the deposition of 0.05% net pyridine in neon. (a) after 10 min of gas deposition at 4 K, (b) after annealing to 12 K, (c) after 15 min of  $280\text{ nm} > \lambda > 250\text{ nm}$  UV light irradiation at 4 K.

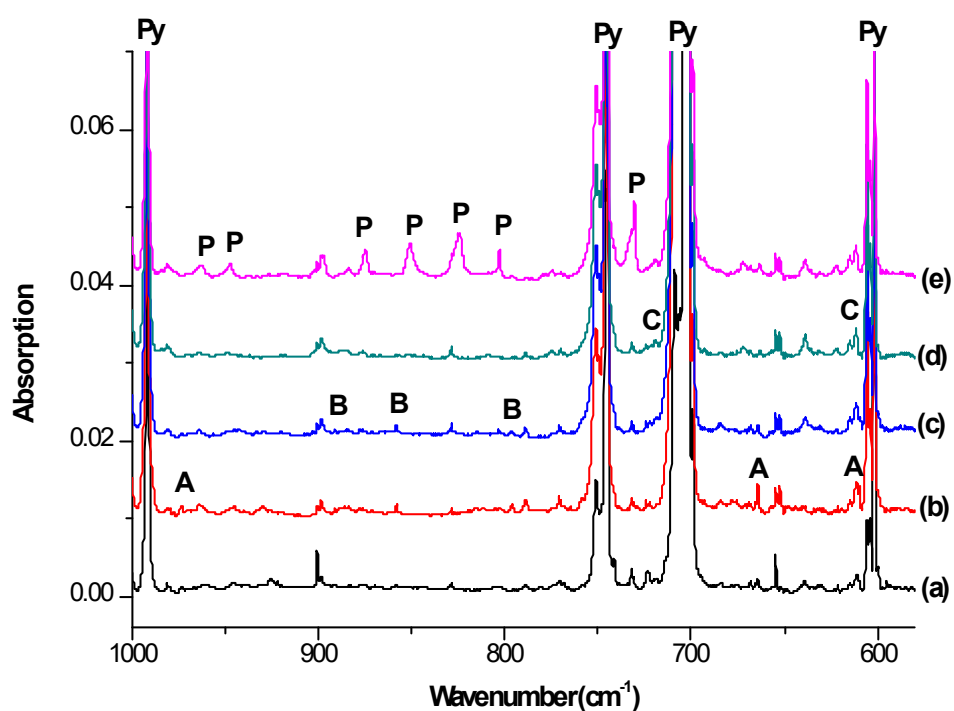


**Figure S2.** Infrared spectra in the  $1000\text{-}580\text{ cm}^{-1}$  region from the co-deposition of  $^{10}\text{B}$  atoms with 0.05% pyridine in neon. (a) after 30 min of sample deposition at 4 K, (b) after annealing to 12 K, (c) after 15 min of visible light ( $495 < \lambda < 580\text{ nm}$ ) irradiation at 4 K, (d) after 15 min of UV-visible light ( $280 < \lambda < 580\text{ nm}$ ) irradiation at 4 K. (e) after 15 min of UV-visible light ( $250 < \lambda < 580\text{ nm}$ ) irradiation at 4 K. **P** represents the photoisomerization product of pyridine. **Py**= pyridine.

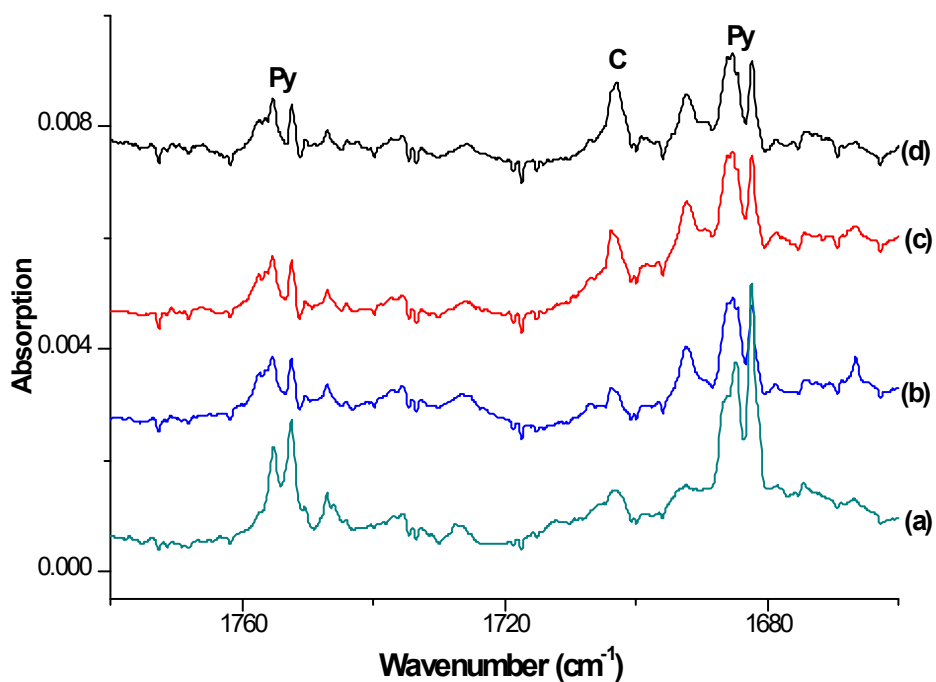


**Figure S3.** Infrared spectra in the 1780-1660  $\text{cm}^{-1}$  region from the co-deposition of  $^{11}\text{B}$  atoms with 0.05% pyridine in neon. (a) after 30 min of sample deposition at 4 K, (b) after annealing to 12 K, (c) after 15 min of visible light ( $495 < \lambda < 580 \text{ nm}$ ) irradiation at 4 K, (d) after 15 min of UV-visible light ( $280 < \lambda < 580 \text{ nm}$ ) irradiation at 4 K.

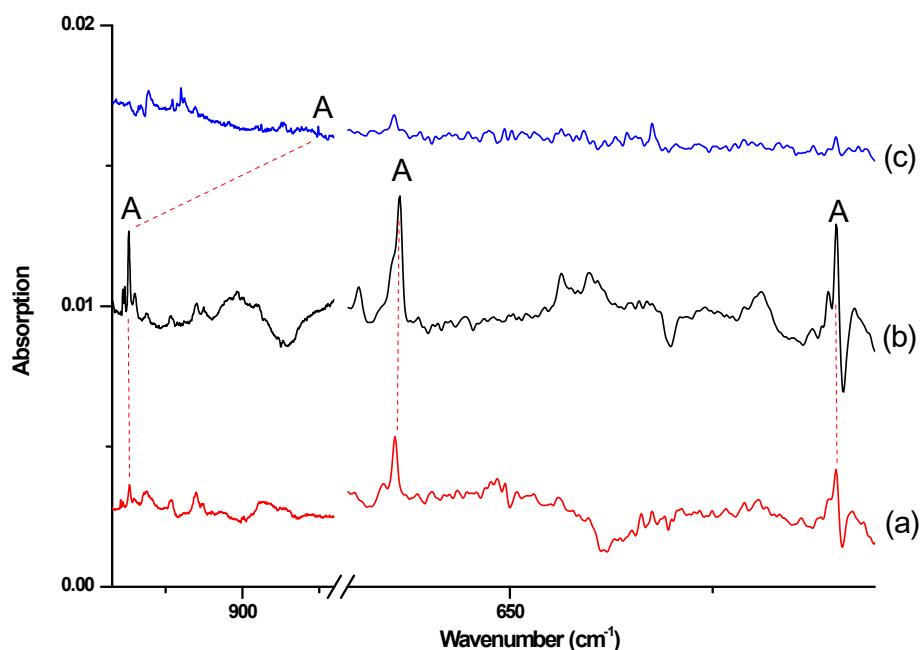


**Figure S4.** Difference spectra in the 1000-600  $\text{cm}^{-1}$  region from co-deposition of boron atoms with isotopic labeled pyridine in solid neon (spectra taken after 12 K annealing minus spectrum after 15 min of  $\lambda > 495 \text{ nm}$  UV light irradiation). (a)  $^{10}\text{B} + 0.05\% \text{ C}_5\text{H}_5\text{N}$ , (b)  $^{11}\text{B} + 0.05\% \text{ C}_5\text{H}_5\text{N}$ , (c)  $^{10}\text{B} + 0.05\% \text{ C}_5\text{D}_5\text{N}$ . The spectra show the variations in the infrared absorption peaks of species A transitioning to C under different isotopic conditions.



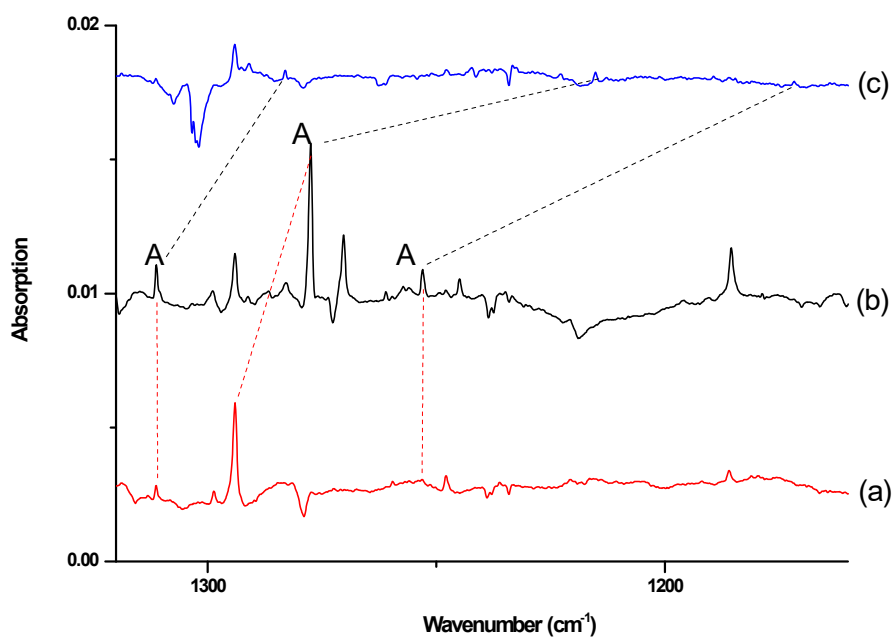


**Figure S5.** Difference spectra in the 1350-1150  $\text{cm}^{-1}$  region from co-deposition of boron atoms with isotopic labeled pyridine in solid neon (spectrum taken after 12 K annealing minus spectrum after 15 min of  $\lambda > 495$  nm UV light irradiation). (a)  $^{10}\text{B} + 0.05\% \text{C}_5\text{H}_5\text{N}$ , (b)  $^{11}\text{B} + 0.05\% \text{C}_5\text{H}_5\text{N}$ , (c)  $^{10}\text{B} + 0.05\% \text{C}_5\text{D}_5\text{N}$ . The spectra show the variations in the infrared absorption peaks of species A transitioning to C under different isotopic conditions.

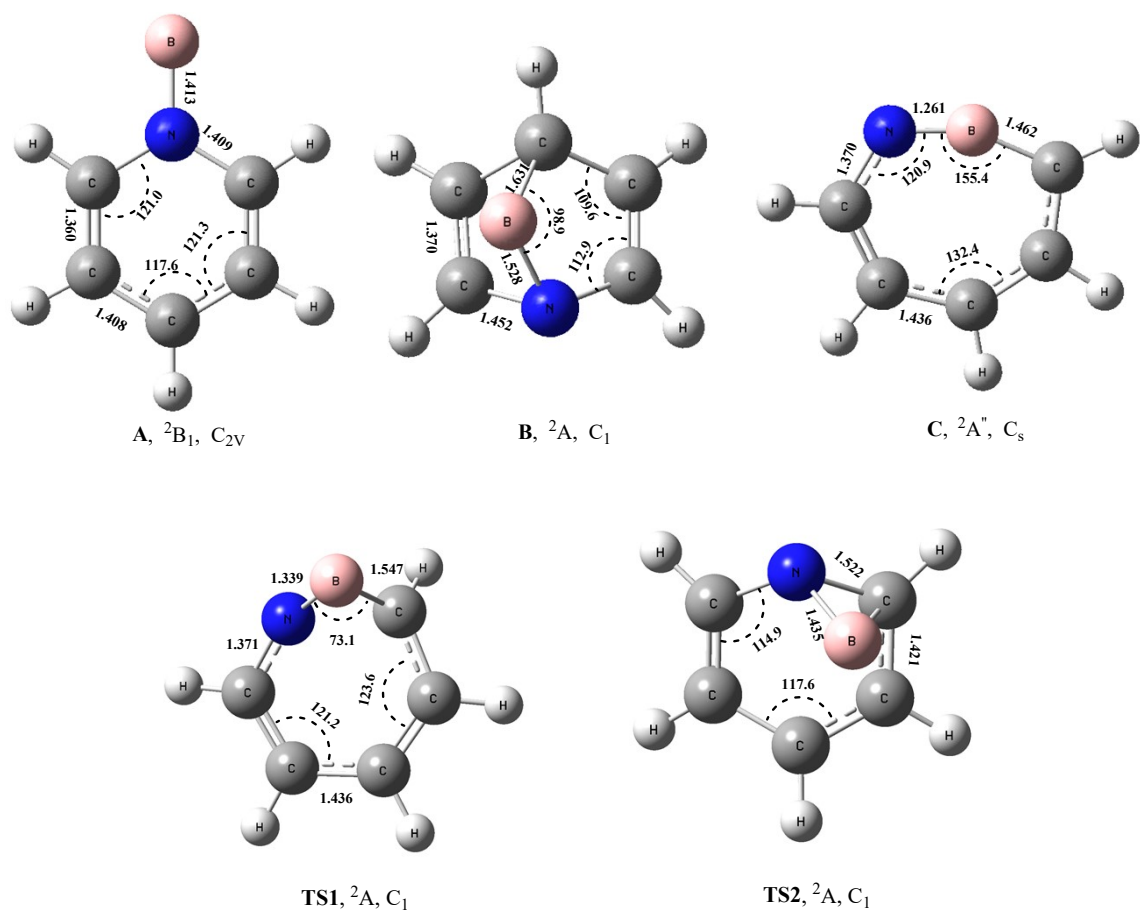


**Figure S6.** Optimized structures of the intermediates and transition states involved in the reaction pathways as shown in figure 6 at the B3LYP/aug-ccpVTZ level. Bond lengths in angstroms and bond angles in degrees.

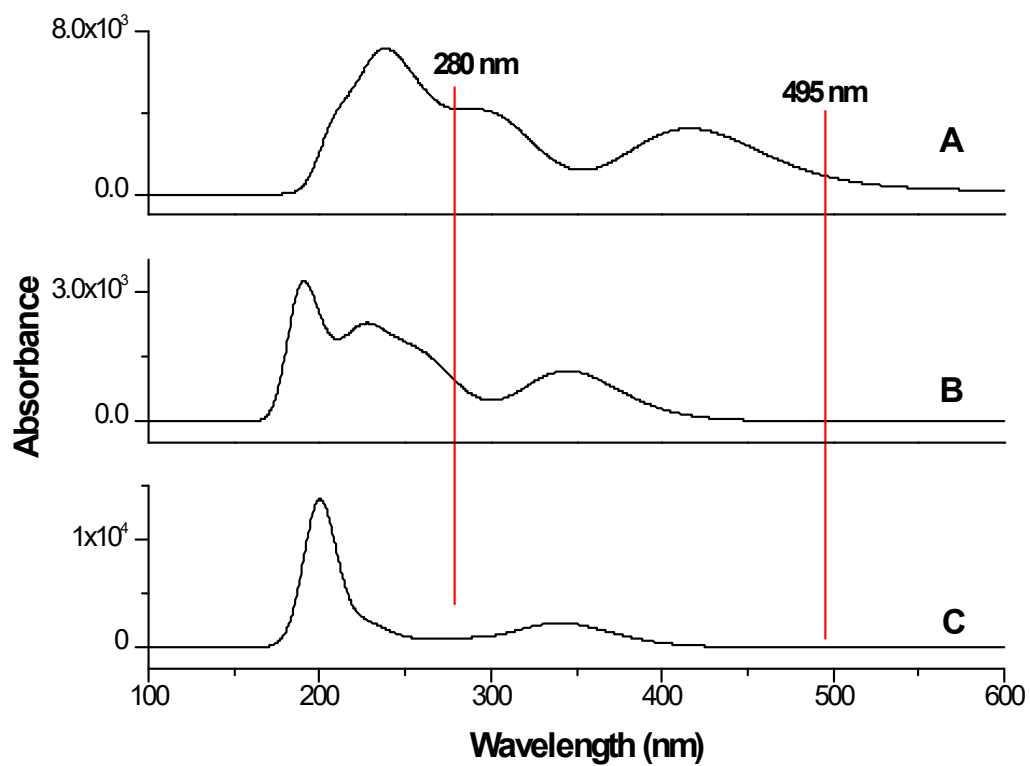


**Figure S7.** The calculated electronic absorptions spectrum of species **A**, **B** and **C** at the B3LYP-TD/aug-cc-pVTZ level of theory.

**Table S6.** Calculated atomic coordinates (in Angstroms) of species **A–C** at the B3LYP/aug-cc-pVTZ level.

(a) **A**, ( $C_{2v}$ ,  ${}^2B_1$ )

C	0.39981800	1.20656600	0.00000100
C	-0.96014600	1.20474800	0.00000000
C	-1.68957900	0.00000000	-0.00000100
C	-0.96014600	-1.20474800	0.00000000
C	0.39981800	-1.20656600	0.00000100
H	0.99369000	2.10676200	0.00000100
H	-1.47092900	2.15744400	-0.00000100
H	-2.76791700	0.00000000	0.00000000
H	-1.47092900	-2.15744400	-0.00000100
H	0.99369000	-2.10676200	0.00000200
B	2.53956800	0.00000000	-0.00000200
N	1.12656600	0.00000000	0.00000100

(b) **B**, ( $C_1$ ,  ${}^2A$ )

C	1.25430200	-0.72972600	-0.19405700
C	1.35758400	0.59575800	-0.21715300
C	0.08069600	1.20929400	0.27187800
C	-1.11237000	0.68369900	-0.47216100
C	-1.13352100	-0.68504700	-0.40824500
H	1.95633100	-1.46950800	-0.54670400
H	2.19472200	1.16911300	-0.58685600
H	0.04754000	2.25799800	0.52669100
H	-1.95847500	1.28920900	-0.76567000
H	-1.95541500	-1.33200400	-0.67736900
N	-0.00732500	-1.18956500	0.35702800
B	-0.58271600	-0.00634300	1.13383000

(c) C, (C<sub>s</sub>, <sup>2</sup>A'')

---

C	0.62010800	-1.28599600	0.00000000
C	-0.81597400	-1.25788400	0.00000000
C	-1.66892900	-0.18490300	0.00000000
C	1.58194000	-0.27054100	0.00000000
C	1.43296200	1.13149600	0.00000000
H	1.03496700	-2.28545200	0.00000000
H	-1.29100900	-2.23135700	0.00000000
H	-2.73803000	-0.36574700	0.00000000
H	2.60591600	-0.63328700	0.00000000
H	2.29142800	1.78018400	0.00000000
B	0.00000000	1.41725200	0.00000000
N	-1.25770200	1.12233900	0.00000000

---